Laser and Particle Beams (2012), *30*, 387–396.

doi:10.1017/S0263034612000225

A method to determine the flux limiter via the motion of the M-band emission region in Au hohlraum

YIQING ZHAO, KE LAN, PENG SONG, WUDI ZHENG, AND XIN LI
Institute of Applied Physics and Computational Mathematics, Beijing, People's Republic of China
(RECEIVED 15 February 2012; ACCEPTED 22 March 2012)

Abstract

In this paper, the influence of the electron flux limiter f_e on hohlraum plasmas is studied by using the two-dimensional code LARED-H, and a method to experimentally determine f_e via the motion of the M-band emission region in Au hohlraum is proposed. From our simulations, the limited free streaming flux may dominates the heat conduction in the regions with steep temperature gradient, including the laser deposition region, the flux-heated overcritical region, and the laser channel boundary between the hot laser plasmas and the surrounding radiation ablated plasmas, while these are important X-ray emission regions. Hence, the choosing of f_e may influence the wall plasma expansion and the laser spot motion, and further influence the motion of the emission regions. From our study, the motion of the M-band (>1.5 keV) emission region is sensitive to f_e when the limited free streaming flux dominates the heat conduction of the wall plasma expansion region, and so it is possible to determine f_e via the motion of the M-band emission region. In this work, the model used in our simulations is taken from the wall and laser spot motion experiments done by Huser *et al.* (2009).

Keywords: Flux limiter; Hohlraums; Plasma expansion

INTRODUCTION

Electron heat conduction plays a major role in inertial fusion physics, because it carries the deposited laser energy from the critical surface to the ablation front (Lindl, 1995; Lindl *et al.*, 2003; Atzeni & Meyer-ter-Vehn, 2004; Gupta & Godwal, 2001). The calculation of the electron transport influences the laser deposition and plasma status inside the hohlraum, it further influences the plasma emission, the laser plasma interaction and the radiation uniformity of the capsule placed in the center of the hohlraum, and finally, it significantly influences the ignition. Therefore, worldwide experimental and theoretical efforts on electron transport in plasmas are in progress (Sunahara *et al.*, 2003; Colombant *et al.*, 2005; Shurtz *et al.*, 2000), especially in recent initial ignition campaign at the National Ignition Facility (Lindl & Moses, 2011; Haan *et al.*, 2011; Rosen *et al.*, 2011). Up to now, various theoretical models have been developed for electron transport, such as the classical electron transport model of Spitzer-Härm (1953; Cohen *et al.*, 1950), the flux limit model (FL model) (Malone *et al.*, 1975), the nonlocal electron transport model (Luciani *et al.*, 1983), and the non-Maxwellian model (Huo *et al.*, 2012). Among all these models, the FL model is the most widely used one in calculating the electron heat flux in hohlraum simulations codes, like LASNEX (Zimmerman & Kruer, 1975), HYDRA (Marinak *et al.*, 1996), FCI2 (Buresi *et al.*, 1986), and LARED-H (Pei, 2007). In the last decades, numerical experiments are designed with FL model (flux limiter) and good results were obtained (Li *et al.*, 2010; Lan *et al.*, 2010, 2004; Cook *et al.*, 2008; Seifter *et al.*, 2009; Orlov *et al.*, 2011). In the FL model, a flux limiter f_e is taken to make sure that the flux does not exceed the limit of the free streaming heat flux Q_f, and the heat flux is often computed either as $\min(Q_{SH}, f_e Q_f)$ or in a "parallel connection" formulation $[Q_{SH}^{-1} + (f_e Q_f)^{-1}]^{-1}$, where f_e is often chosen from 0.05 to 0.15 (Atzeni & Meyer-ter-Vehn, 2004; Rosen & Nuckolls, 1979; Kline *et al.*, 2011). In recent theoretical work done for the National Ignition Campaign (Rosen *et al.*, 2011), a flux limiter of 0.15 was finally taken in the ignition design after comparing with the nonlocal model. However, the choice of f_e depends on the hohlraum and the laser parameters used in the study. Hence, it is necessary to find a way to determine f_e experimentally for different designs.

Address correspondence and reprint requests to: Yiqing Zhao, Institute of Applied Physics and Computational Mathematics, P.O. Box 8009-14, Beijing 100088, People's Republic of China. E-mail: yqzhaostudio@gmail.com

In fact, the heat flux may be dominated by the limited free-stream flux in the regions with a steep temperature gradient, including the laser deposition region, the flux-heated overcritical region, and the laser channel boundary between the hot laser plasmas and the surrounding radiation ablated plasmas, while these are important X-ray emission regions. As a result, the choice of f_e may influence the laser spot motion and the wall plasma expansion, and therefore influence the motion of the emission regions. Therefore, it is possible to determine f_e via the diagnostics of the X-ray emissions. In this paper, we will study the influence of the electron flux limiter f_e on hohlraum plasmas by using a two-dimensional (2D) radiation hydrodynamics code LARED-H, and we will propose a method to experimentally determine f_e via the motion of the M-band (>1.5 keV) emission region in Au hohlraum.

The hohlraum and laser parameters used in this study are taken from the experiments done by Huser *et al.* (2009). In their experiments, the authors measured the wall and laser spot motion in the empty, propane filled, and CH-lined Au hohlraums on the Omega laser facility, and compared the experimental results with their simulations with the 2D radiation hydrodynamics code FCI2. Huser *et al.* (2009) observed the wall motion by using axial 2D X-ray imaging and observed the laser spot motion perpendicularly through a thinned wall using streaked hard X-ray imaging. Their experiments gave valuable quantitative results, which are worthy to be compared with the 2D simulations. We will mainly simulate the empty hohlraum used in the experiments (Huser *et al.*, 2009) with different f_e and choose a suitable f_e by comparing our simulations with the observed motion of the X-ray emission regions. Using the chosen f_e, we will also simulate the gas-filled hohlraum used in the experiments of Huser *et al.* (2009) and study the effect of gas filling on the wall plasma expansions.

The paper is organized as follows. In Section 2, we will introduce the code and model used in our study. In Section 3, we will use the LARED-H to simulate the empty hohlraum used in Huser's *et al.* (2009) experiments with different f_e and study the influence of f_e on plasma status. In Section 4, we will study the influence of f_e on the X-ray emission region in the overcritical plasmas. In Section 5, we will study the influence of f_e on the X-ray emission from the plasma corona. In above simulations and discussions, we mainly focus on the empty hohlraum. In Section 6, we study the effect of gas filling on the wall plasma expansion in the gas-filled hohlraum used in Huser's *et al.* (2009) experiments. Finally, we will present a summary in Section 7.

2. CODE AND MODEL

The LARED-H is a 2D radiation hydrodynamics code for laser target coupling and hohlraum physics study, which is one of the main simulation codes in designing and analyzing the hohlraum experiments on SGII and SGIII Prototype laser facilities (Li *et al.*, 2011; Huo *et al.*, 2010). The three-temperature hydrodynamic equations in LARED-H are:

$$\frac{\partial \rho}{\partial t} + \nabla \cdot (\rho \mathbf{u}) = 0, \tag{1}$$

$$\rho \frac{d\mathbf{u}}{dt} + \nabla (P_e + P_i + P_r + q) = 0, \tag{2}$$

$$C_{ve} \frac{dT_e}{dt} = W_{pe} + W_{fe} + W_l + W_{er} + W_{ei}, \tag{3}$$

$$C_{vi} \frac{dT_i}{dt} = W_{pi} + W_{fi} - W_{ei}, \tag{4}$$

$$\frac{d}{dt}\left(\frac{E_r}{\rho}\right) = W_{pr} + W_{fr} - W_{er}. \tag{5}$$

Here, the subscripts e, I, and r indicate electron, ion, and radiation, respectively; the symbol ρ denotes the mass density, $\mathbf{u}$ is the flow velocity; T is the temperature; P is the pressure, and q is the artificial viscosity; C_{ve} and C_{vi} are the specific heats of free electron and ion, respectively; W_p is the work term due to pressure; W_f is the thermal conduction term; W_{er} is the electron-radiation energy exchange term; W_{ei} is the electron-ion energy exchange term; and E_r is the radiation energy density; W_l is the laser energy deposition via inverse bremsstrahlung and is calculated with a three-dimensional ray-tracing package. An average-atom atomic physics model is included in the code, and the following atomic processes are involved: (1) collisional excitation and de-excitation, (2) spontaneous emission, (3) collisional ionization and three-body recombination, (4) photon ionization and radiative recombination, (5) dielectron capture and auto-ionization.

The expressions of the above energy terms are:

$$W_{fe} = -\frac{1}{\rho} \nabla \cdot \mathbf{F_e}, \tag{6}$$

$$W_{fi} = -\frac{1}{\rho} \nabla \cdot \mathbf{F}_i, \tag{7}$$

$$W_{fr} = -\frac{1}{\rho} \nabla \cdot \mathbf{F}_r, \tag{8}$$

$$W_{pe} = -P_e \frac{d}{dt}\left(\frac{1}{\rho}\right), \tag{9}$$

$$W_{pi} = -(P_i + q) \frac{d}{dt}\left(\frac{1}{\rho}\right), \tag{10}$$

$$W_{pr} = -P_r \frac{d}{dt}\left(\frac{1}{\rho}\right), \tag{11}$$

$$W_{ei} = 4\sqrt{\frac{2\pi m_e}{k_B}} \frac{N_e N_i}{\rho} \times \frac{e^4 z^2}{m_i} \times \frac{T_e - T_i}{T_e^{3/2}} \times \ln \Lambda_{ei} \tag{12}$$

$$W_{er} = W_{fb} + W_{bb} + W_{ff}, \tag{13}$$

Here, m_e is the electron mass; m_i is the ion mass; e is the electron charge; ln Λ_{ei} is the Coulomb logarithm for collisions between electrons and ions; k_B is the Boltzmann constant; z is the average ionization degree; N_i is the ion density, and

https://doi.org/10.1017/S0263034612000225 Published online by Cambridge University Press

N_e is the electron density; W_{bf}, W_{bb}, and W_{ff} represent the energy exchanges due to free-bound, bound-bound and free-free transitions of atomic processes, respectively. The electron heat flux $\mathbf{F}_e$ taken in our code is the minimum of the S-H flux[11] F_{SH} and the limited free-stream heat flux f_eF_l, here F_l is the free-stream heat flux.

In LARED-H, the thermodynamic quantities are derived either from the ideal gas model or from data of realistic equation of state. The mean opacity is calculated with relativistic F_{SH} self-consistent average-atom-model OPINCH (Serduke *et al.*, 2000) where the contributions from free-free, free-bound, and bound-bound transitions are taken into account.

We had used LARED-H to simulate the laser spot moving experiment on NOVA[2]. In the experiment, a 1 ns flat-top laser pulse was used to drive a hohlraum of 2500 μm in length and 1600 μm in diameter with one laser entrance hole of 800 μm diameter at each end. From LARED-H, the relationship between the laser power P_L and the angular velocity $d\theta/dt$ of the emission center seen by capsule is $d\theta/dt = 5.7°/ns + 3.2°/ns(\log_{10} P_L)$, which is obtained by using the least square method.

In this work, the hohlraum and laser parameters used are taken from the experiments done by Huser *et al.* (2009). Both empty and propane-filled hohlraums are considered. The cylindrical Au hohlraum is 1.5 mm long with 1.6 mm diameter, with a full-open laser entrance hole at each end. The hohlraum wall thickness is taken as 25 μm. The laser pulse of about 9.5 kJ in total has the shape of Omega PS26N01A with 1 ns pre-pulse followed by 1.5 ns main-pulse with 5:1 contrast. The thirty laser beams simultaneously irradiate the hohlraum from two ends, with respectively, 10 beams at an incidence cone of 42° angle and 20 beams at 59° angle. In our 2D simulations, the widths of both laser rings at 42° and 59° are taken as 400 μm on the inner wall of hohlraum. The laser rings at 42° from two sides not only overlap each other at the hohlraum center, but also overlap the rings at 59° from the same side at about $z = 200$ μm. Here, z is the axial position from hohlraum center. Thus, the middle part of the hohlraum wall, around 600 μm in length, is fully under the irradiation of the laser. In addition, the initial width of the first Lagrangian cell on the inner surface of wall is taken as 10 nm and the initial temperature of the hohlraum is taken as 300 K. For the empty hohlraum, a pseudo-gas of Au with 8×10^{-4} g/cm^3 initial density is used, and it is assumed that there is no laser deposited in the pseudo-gas. For the X-ray emissions, same as in the experiments (Huser *et al.*, 2009), we also focus on O-band (about 450 eV), N-band (about 800 eV) and M-band (>1.5 keV) and use the same spectral responses for these three bands.

3. HOHLRAUM PLASMA STATUS UNDER DIFFERENT FLUX LIMITERS

The electron conduction carries the deposited laser energy from the critical surface to the over-critical plasma and the plasma corona, so the calculation of the heat conduction influences the plasma status and the X-ray emissions inside hohlraum. In this section, we study the 2D simulation results of the empty hohlraum model and compare the hohlraum plasma status under different f_e. From our simulations, the results are sensitive to f_e when f_e is smaller than 0.1, but insensitive when $f_e > 0.1$. Therefore, we mainly present below the results with $f_e = 0.05$ and 0.1.

First, one should know in which regions the heat conduction is limited by the flux limiters inside hohlraum. In Figure 1, we present the 2D maps of the laser energy deposition term W_l and the areas in which the heat flux is dominated by the limited free-stream flux f_eF_l with respective to f_e of 0.05 and 0.1, at 1 ns when the pre-pulse ends while the main pulse starts. The pulse shape of drive laser is also presented in Figure 1a. As shown, the heat flux is dominated by f_eF_l in the regions with steep temperature gradient, including the laser deposition region, over-critical plasma region and the laser channel boundary between the hot laser plasmas and the surrounding radiation ablated plasmas, which are important regions for the X-ray emissions. However, the limited regions are narrower at a higher f_e. When f_e is taken as 0.2, from our simulations, the heat conduction is mainly dominated by the S-H flux almost in the whole hohlraum. Notice that f_eF_l dominates the heat conduction also in the pseudo-gas and at the boundary between the pseudo-gas and the laser channel, but we do not concern these regions that are related to the pseudo-gas in this paper. From our simulation, the plasma-filling is not serious even at the peak laser time. Thus, the laser is mainly deposited near wall for this model.

Now, we study and compare the plasma status along the laser channel under different f_e. Because the laser energy at the 59° angle is two times as large as that at the 42°, so we mainly focus on the laser channel at 59°. In Figures 2 and 3, we present the distributions of T_e, n_e, and ionization degree Z_{eff} along the laser channel at 59° at 1.7 ns, just after the laser begins to fall and the radiation temperature T_r in the hohlraum reaches its peak. As shown, the maximum T_e at $f_e = 0.05$ is about 400 eV higher than at $f_e = 0.1$, Z_{eff} at R_c is about 1.5 higher, and both R_c and the ionization front are around 10 μm closer to wall. Here, R_c is defined as the critical position at $n_e/n_c = 1$. The reason for a higher maximum T_e at a smaller f_e is that less energy is conducted to the over-critical region and less mass ablated from wall when the heat conduction is more limited. As a result, at a smaller f_e, the laser ablated plasmas are hotter and expand faster along the radial direction, resulting in a lower n_e in the plasma corona. Obviously, the critical position and the ionization front move slower towards the hohlraum axis at a smaller f_e.

In Figure 4, we present the temporal n_e of the Lagrangian cells that produce respective maximum emissions of the three bands at $f_e = 0.05$ and 0.1. As shown, for both flux limiters, during the whole laser driving, the maximum emissions of N-band and O-band are generated at the same positions in

https://doi.org/10.1017/S0263034612000225 Published online by Cambridge University Press

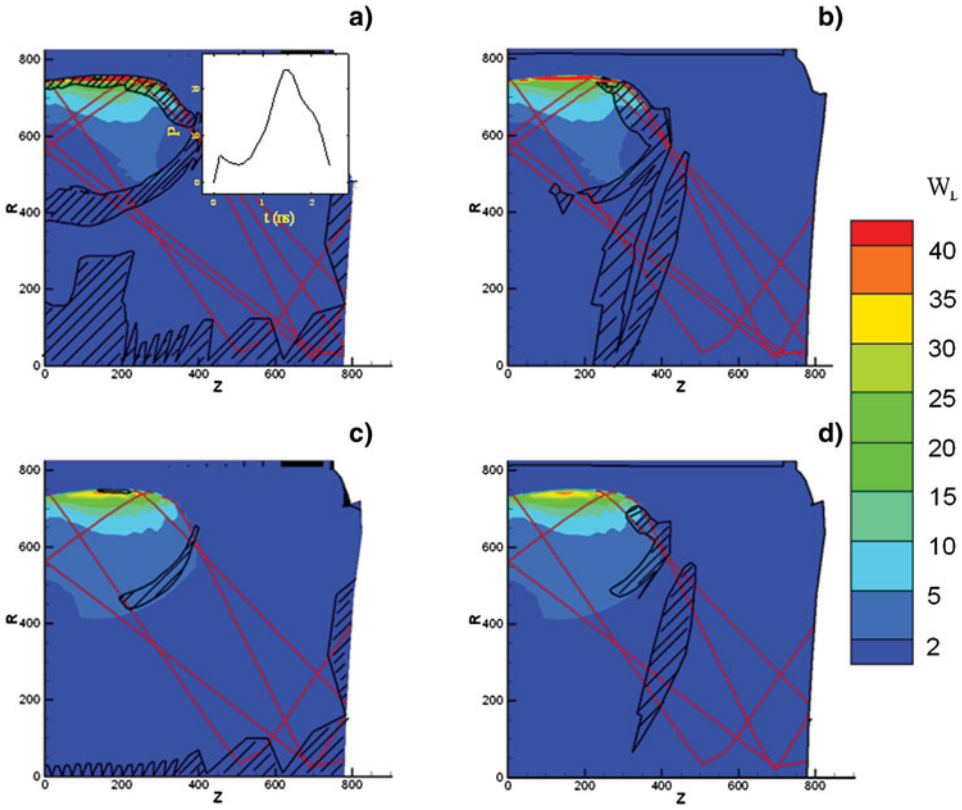

Fig. 1. (Color online) 2D maps of the laser energy deposition term W_l (10^{15} W/m^3) and the areas in which the heat flux is dominated by $f_L F_l$ along, respectively, the $\hat{l}$ direction (**left images**) and the $\hat{k}$ direction (**right images**), at 1 *ns* with $f_e = 0.05$ (**upper images**) and 0.1 (**lower images**), in which the red lines represent the laser pass. The directions of $\hat{l}$ and $\hat{k}$ are defined for 2D simulation, which are time-dependent and related to cells. The initial directions of $\hat{l}$ and $\hat{k}$ are in $\hat{r}$ and $\hat{z}$, respectively. The inner plot in (a) is the pulse shape of drive laser.

the overcritical region, $n_e \approx 2$–4 during the main laser pulse, while the maximum emissions of M-band are generated in the laser deposited region with $n_e < 1$. From our simulations, the value of f_e influences not only the peaks of the O-band, N-band, and M-band emissions, but also the positions of the emission regions. As shown in Figure 5, compared to the results at $f_e = 0.1$, the peaks of O-band, N-band, and M-band are about, respectively, 50%, 100%, and 200% higher at $f_e = 0.05$ and the peak positions for all three bands are around 10 μm closer to wall. Therefore, we can

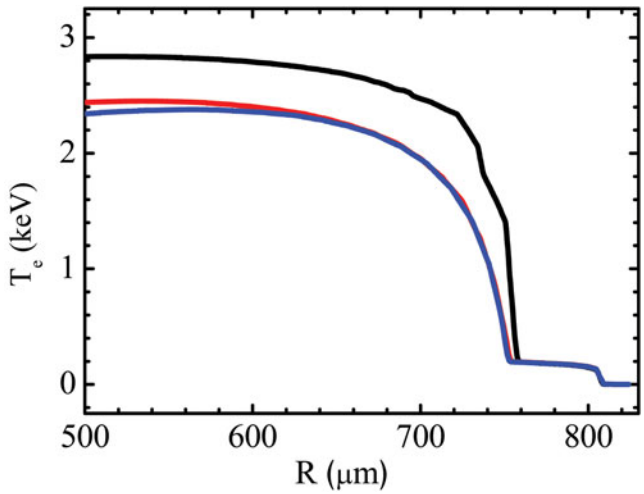

Fig. 2. (Color online) The distributions of T_e along the laser pass of the 59° beams at 1.7 ns with f_e of 0.05 (black), 0.1 (red) and 0.2 (blue).

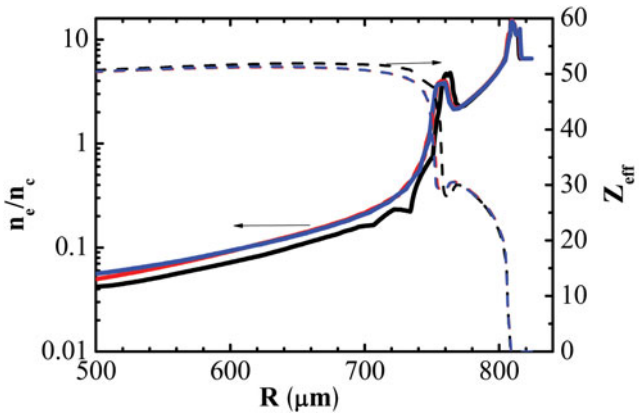

Fig. 3. (Color online) The distributions of n_e (solid) and Z_{eff} (dashed) along the laser pass of the 59° beams at 1.7 ns with f_e of 0.05 (black), 0.1 (red) and 0.2 (blue).

https://doi.org/10.1017/S0263034612000225 Published online by Cambridge University Press

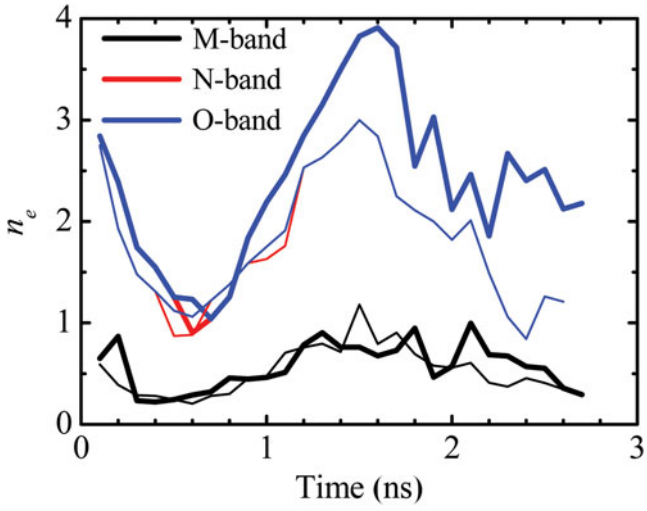

Fig. 4. (Color online) The temporal n_e of the Lagrangian cells which produce, respectively, the maximum M-band (black), N-band (red) and O-band (blue) emissions inside hohlraum, with $f_e = 0.05$ (thick lines) and $f_e = 0.1$ (thin lines). The curve of N-band almost overlaps with O-band during whole time.

determine f_e for a hohlraum design via the X-ray emissions from experiments.

We also study the influence of f_e on the hohlraum T_r, the laser absorption efficiency η_L and the laser X-ray conversion efficiency η_X. Shown in Figure 6 are variations of η_L, η_X, and the post-processed T_r along the line 40° from hohlraum axis through LEH as f_e at the peak laser time 1.7 ns. For η_L, it is about 1 at $f_{e \geq 0.05}$, while it decreases to 94% at $f_{e = 0.03}$. The reason is that the laser deposition is lower in a hotter hohlraum generated with a smaller f_e, thus more laser energy escapes from the two LEHs. For η_X, it increases as f_e, because more mass is ablated and emits at a larger f_e. As shown, η_X is 70% at $f_e = 0.03$ and increases to 80% after $f_e \geq 0.07$. For T_r,

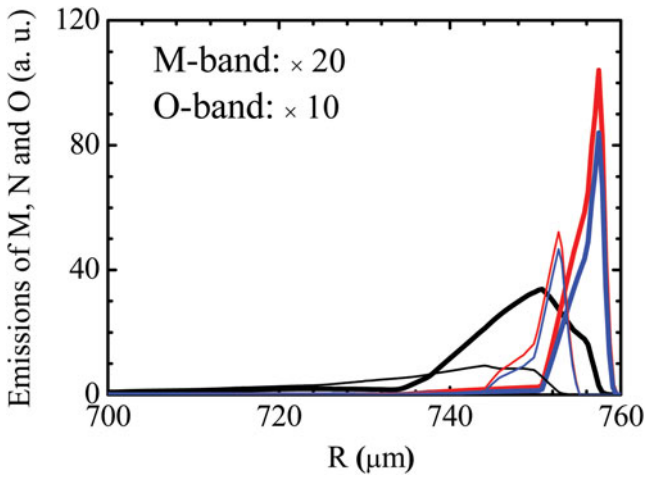

Fig. 5. (Color online) The distributions of M-band (black), N-band (red) and O-band (blue) emissions along the laser pass of the 59° beams at 1.7 ns with f_e of 0.05 (thick) and 0.1 (thin).

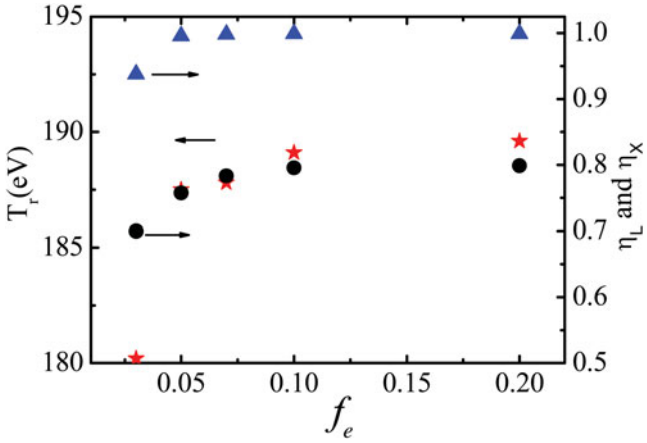

Fig. 6. (Color online) Variations of T_r (red star), η_L (blue triangle) and η_X (dark circle) as f_e at 1.7 ns.

it increases as f_e because of higher η_L and η_X at a larger f_e. Nevertheless, the variation of T_r is small, just within 3 eV when $f_e \geq 0.05$. As shown, T_r is about 188 eV from LARED-H with $f_e = 0.07$, which agrees with the experimental observations (Huser *et al.*, 2009).

4. INFLUENCE OF F_E ON THE X-RAY EMISSION REGION IN OVERCRITIAL PLASMAS

In this section, we study the influence of f_e on the motion of the X-ray emission region in the overcritical plasmas, which is often observed through a thinned wall hohlraum by a camera in experiments. Same as Huser *et al.* (2009) we also define the axial centroid position of emission intensity as:

$$z_I = \frac{\int I(z')z'dz}{\int I(z')dz},$$

where $I(z)$ is the post-processed emission intensity for whole spectrum observed from the hohlraum axis along the radial direction. Moreover, we define the axial centroid velocity as $v_I = dz_I/dt$. In Figure 7, we present the simulated temporal relative displacements of z_I under different f_e for the empty hohlraum and compare them with the experimental observations. As shown, the emission region moves slower with a smaller f_e, which reason will be discussed below. From 1 ns to 2 ns, the experimental results are between the simulations with flux limiter of 0.05 and 0.07, with v_I being about 55 μm/ns. However, after 2.0 ns when the main laser pulse falls rapidly, v_I is about 205 μm/ns from our simulations, much higher than the experimental observations of 55 μm/ns. We still cannot understand this big difference between the simulations and the observations.

In order to understand why the emission region moves slower with a smaller f_e, we present in Figure 8 the electron pressure P_e along the center line of the laser channel. As shown, there are two peaks of P_e, at about 760 μm and at

https://doi.org/10.1017/S0263034612000225 Published online by Cambridge University Press

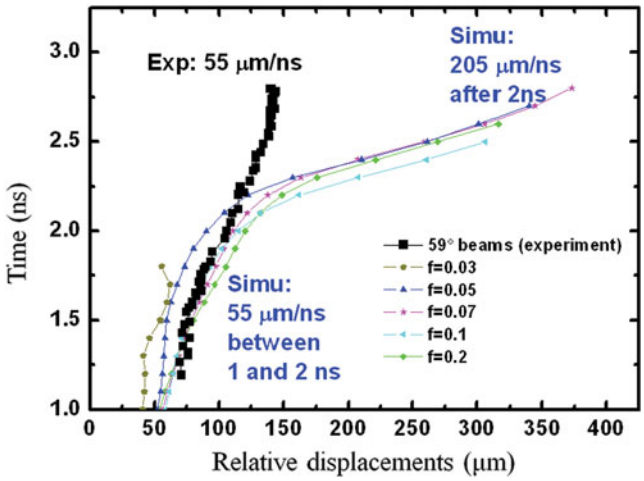

Fig. 7. (Color online) Comparisons of the simulated temporal relative displacements of z_l under different f_e with the experimental observations (Huser *et al.*, 2009) for the empty hohlraum. Here, v_l in blue is obtained from simulations, in black is observed from experiments for the laser beams injected at 59°. Notice that the comparisons start from 1 ns in this figure and the following figures, because there is no experimental data before 1 ns.

about 810 μm. The first peak at 760 μm is caused by the laser ablation. As is known from Figure 2, T_e in the laser ablation region is higher at a smaller f_e, which therefore drives a higher laser ablation P_e. The second peak at about 810 μm is caused by the radiation ablation. The radiation ablation P_e is mainly decided by T_r, while T_r changes little as f_e when $f_e \geq 0.05$, as discussed above. Hence, the radiation ablation P_e is also changes little as f_e when $f_e \geq 0.05$. The motion of the X-ray emission region is decided by the difference between the radiation ablation pressure and the laser ablation pressure. Because the pressure difference is smaller at a smaller f_e, so the motion of the X-ray emission region is slower. Nevertheless, we can see that the motion of the X-ray emission region in overcritical region is somewhat insensitive to f_e for this model.

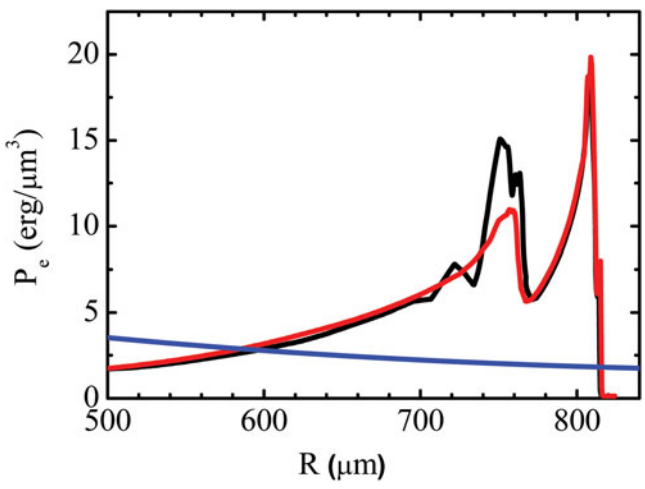

Fig. 8. (Color online) The distributions of P_e at 1.7ns along the laser channel with f_e of 0.05 (black), 0.1 (red) and 0.2 (blue).

5. INFLUENCE OF F_E ON THE X-RAY EMISSION REGION IN PLASMA CORONA

As the laser ablating, the plasma corona inside hohlraum expands toward to the axis. The on-axis imaging of the different X-ray bands were diagnosed by Huser *et al.* (2009). In their work, a free radius $r_{free} = r\,(I = I_{center} + (I_{max} - I_{center})/2)$ is defined to describe the plasma expansion, where I_{center} is the residual intensity at the axis of the hohlraum and I_{max} is the maximum intensity along the radial direction. In order to compare with their observations, we also define such free radii, denoted as $r_{free}^{\text{O-band}}$, $r_{free}^{\text{N-band}}$ and $r_{free}^{\text{M-band}}$ for O-band, N-band and M-band, respectively. The corresponding velocities are denoted as $v_{free}^{\text{O-band}} = dr_{free}^{\text{O-band}}/dt$, $v_{free}^{\text{N-band}} = dr_{free}^{\text{N-band}}/dt$, and $v_{free}^{\text{M-band}} = dr_{free}^{\text{M-band}}/dt$.

We compare our simulations of the temporal $r_{free}^{\text{O-band}}$, $r_{free}^{\text{N-band}}$, and $r_{free}^{\text{M-band}}$ at different f_e with those from the experimental observations in Figure 9. The simulation results from FCI2 (Huser *et al.*, 2009) are also presented for comparison.

For O-band, as shown, all simulations from LARED-H with different f_e are located within the experimental error bars. For the N-band, however, the simulated expansion velocity from both LARED-H and FC12 are obviously faster than the experimental results. We cannot explain this disagreement, but we will check our simulations through a laser spot motion experiment to be done on SGIII-prototype in near future. As shown, the influence of f_e on $r_{free}^{\text{O-band}}$ and $r_{free}^{\text{N-band}}$ are not remarkable, because they are very near to R_c and R_c changes little as f_e from Figure 3. In other words, it is hard to decide f_e from $r_{free}^{\text{O-band}}$ and $r_{free}^{\text{N-band}}$ experimentally.

For M-band, however, the influence of f_e on $r_{free}^{\text{M-band}}$ is more remarkable than for other two bands, and $v_{free}^{\text{M-band}}$ is faster at a smaller f_e, as shown in Figure 9c. The reason is that the M-band is mainly emitted from the hot plasmas ablated by laser, while T_e of the hot plasmas is higher at a smaller f_e, as discussed in the last section. As a result, the expansion velocity of the M-band emission region is faster at a smaller f_e. As shown, the simulation results with $f_e = 0.03$ and 0.05 are beyond the experimental error bars, and the best agreement generates at $f_e = 0.07$.

The variation of v_{free} as f_e is presented in Figure 10 for the three bands. As discussed above, $v_{free}^{\text{O-band}}$ and $v_{free}^{\text{N-band}}$ changes little with f_e while $v_{free}^{\text{M-band}}$ obviously decreases as f_e. As presented, $v_{free}^{\text{M-band}}$ drops from 390 to 150 μm/ns when f_e is changed from 0.03 to 0.2, and $v_{free}^{\text{M-band}}$ is 230 μm/ns at $f_e = 0.07$. Moreover, $v_{free}^{\text{O-band}}$ and $v_{free}^{\text{N-band}}$ are much smaller than $v_{free}^{\text{M-band}}$, and the best agreement between the LARED-H simulations and the experimental observation is at $f_e = 0.07$. Due to the sensitivity of the motion of the M-band emission region to f_e, we therefore propose a method to experimentally determine f_e via the diagnostics of the temporal evolutions of the M-band emission region in plasma

https://doi.org/10.1017/S0263034612000225 Published online by Cambridge University Press

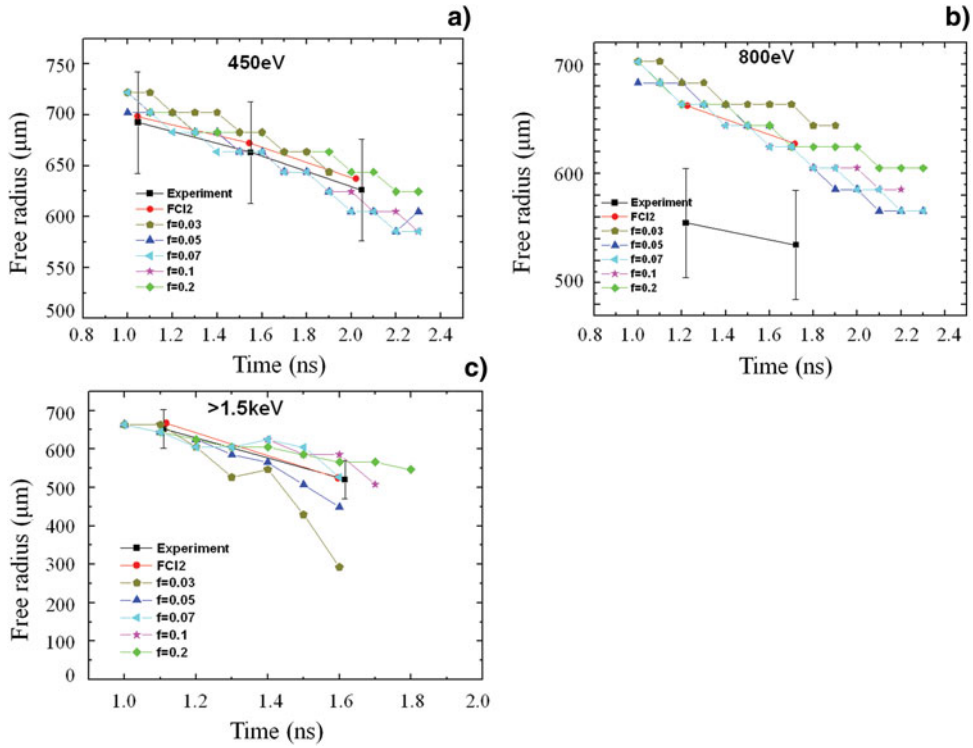

Fig. 9. (Color online) Comparisons of the temporal $r_{free}^{\text{O-band}}$ **(a)**, $r_{free}^{\text{N-band}}$ **(b)** and $r_{free}^{\text{M-band}}$ **(c)** in the empty hohlraum at different f_e with those from the experimental observations (with black square) and the simulations from FCI2 (with red circle) (Huser *et al.*, 2009). The free radii are postprocessed results from LARED-H simulations along the hohlraum axis.

corona inside a Au hohlraum which has strong M-band emissions under drive conditions concerned in indirect-drive inertial fusion study.

It is also possible to measure the X-ray emission region in plasma corona from LEH, but a suitable angle should be chosen for observation. Presented in Figure 11 is the X-ray emission intensity map and the contour line of $\rho = 0.05$ g/cm^3 at the laser power peak time 1.7 ns. In the region above the yellow line, there is $\rho > 0.05$ g/cm^3. As shown, the maximum X-ray emission area is located at $r \approx 770$ μm and $z \approx 200$ μm. Between the X-ray emission region and the LEH, it is the radiation ablated plasmas, which are about 400 μm in length with $\rho = 0.05$ g/cm^3 and $T_r \approx 200$ eV. From our opacity model, the Rosseland mean free paths at $T_r \approx 200$ eV and $\rho_e = 0.05$ are 56.55 μm × 6.23 μm and 46.50 μm, respectively, $h\nu = 400$ eV, 800 eV, and 1.5

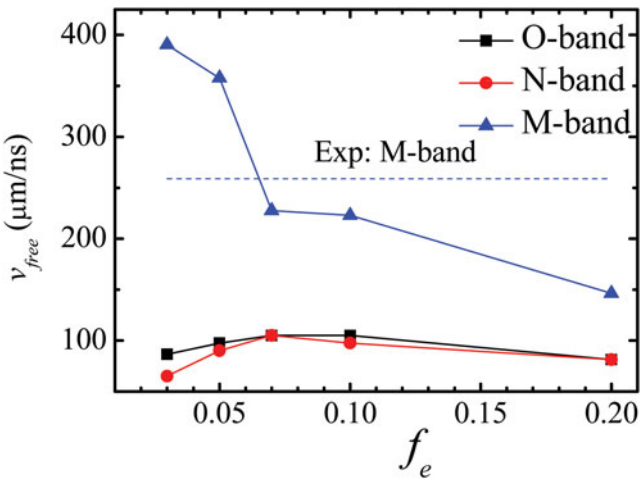

Fig. 10. (Color online) Variations of v_{free} as f_e for O-band (black), N-band (red) and M-band (blue).

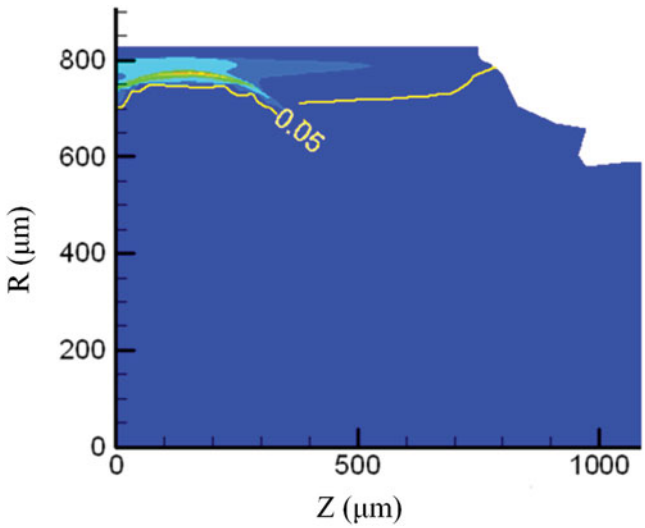

Fig. 11. (Color online) The X-ray emission intensity map and the contour line of $\rho = 0.05$ g/cm^3 at 1.7 ns, with $f_e = 0.05$.

https://doi.org/10.1017/S0263034612000225 Published online by Cambridge University Press

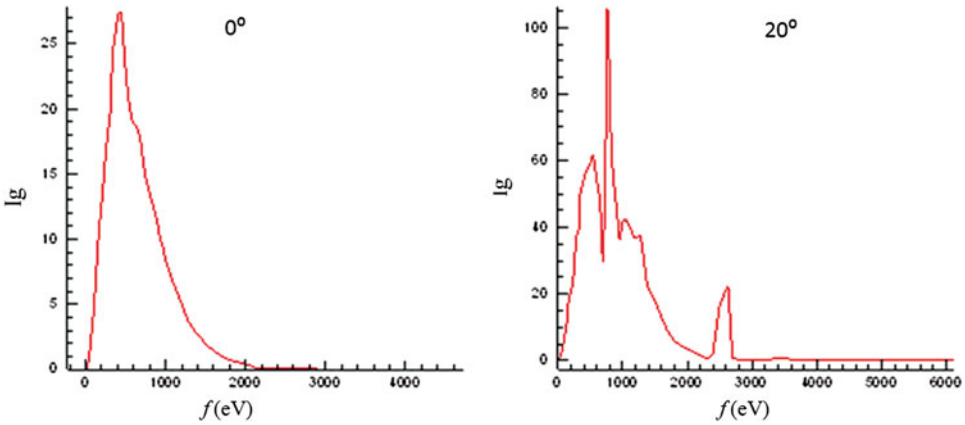

Fig. 12. (Color online) The postprocessed x-ray flux spectrum along the lines at 0°and 20° from the Hohlraum axis through LEH at 1.7 ns, with $f_e = 0.05$.

keV, which are much shorter than 400 μm. Hence, the radiation ablated plasmas are optically thick. Presented in Figure 12 is the postprocessed X-ray flux spectrum along the line 0°and 20° from the Hohlraum axis through LEH. As shown, the spectrum observed at 0° through the optically thick plasmas is very near to the Planckian distribution, while at 20° the structures of O-band, N-band and M-band from the X-ray emission region near the laser deposited region can be clearly observed from the spectrum. Therefore, an observation angle should be carefully chosen to measure the emissions near the laser spot region through LEH. Together with the measurement of the X-ray emissions along the axial direction, it is possible to obtain the motion of the X-ray emission region along the radial direction.

6. THE EFFECT OF GAS FILLING ON THE WALL PLASMA EXPANSION

To hold back the wall plasma expansion and to ensure that the laser beams propagate to positions near the hohlraum wall, a gas-filled hohlraum is usually used in inertial fusion study. In the experiments done by Huser *et al.* (2009) the authors also measured the wall and laser spot motion in a propane-filled hohlraum. In this section, we take f_e as 0.07

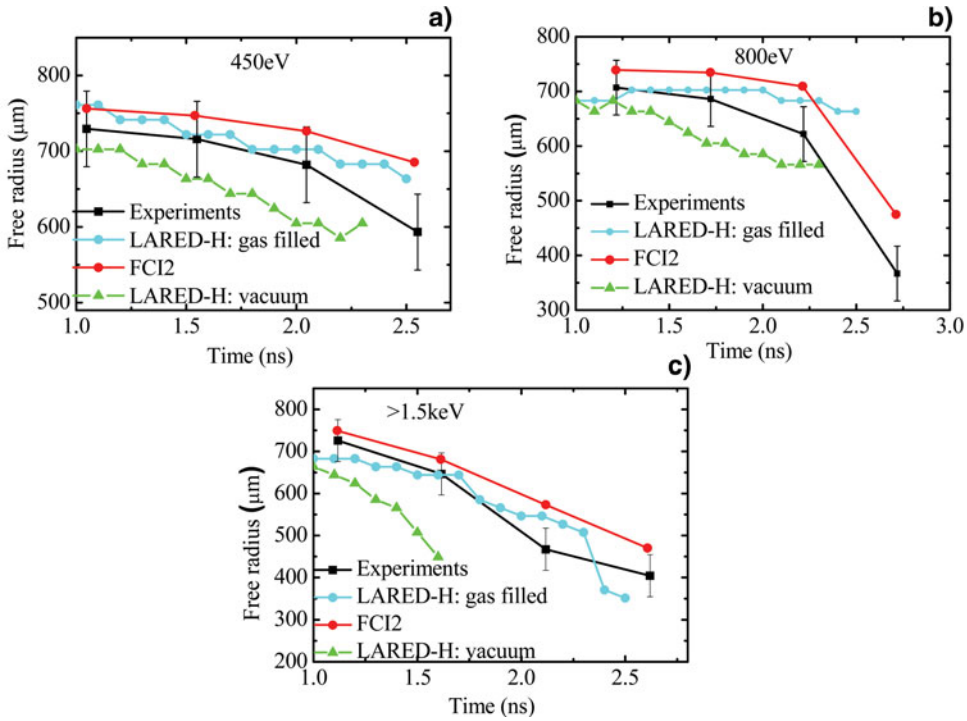

Fig. 13. (Color online) Comparisons of the temporal $r_{free}^{\text{O-band}}$ (**a**), $r_{free}^{\text{N-band}}$ (**b**), and $r_{free}^{\text{M-band}}$ (**c**) in the gas-filled hohlraum at $f_e = 0.07$ with those from the experimental observations (with black square) and the simulations from FCI2 (with red circle). The LARED-H results for the empty hohlraum are also presented for comparison.

https://doi.org/10.1017/S0263034612000225 Published online by Cambridge University Press

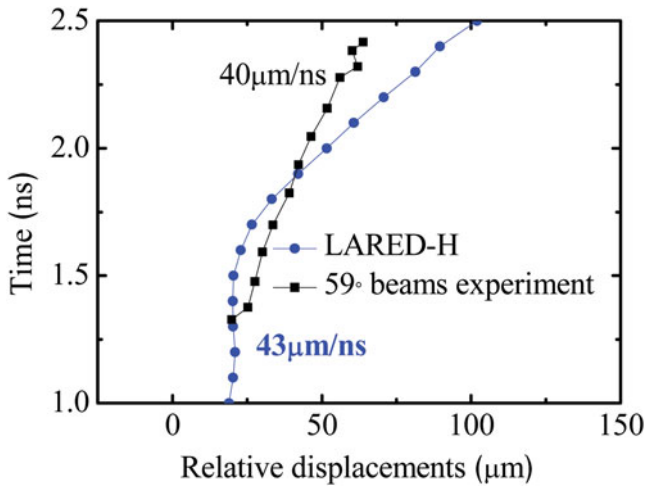

Fig. 14. (Color online) Comparisons of the simulated temporal relative displacements z_I at $f_e = 0.07$ with the experimental observations for the gas-filled hohlraum. Here, v_I in blue is obtained from simulations, in black are observed from experiments (Huser *et al.*, 2009) for the laser beams injected at 59°.

and compare our simulations with the observations (Huser *et al.*, 2009).

In Figure 13, we present the LARED-H simulations of the temporal $r_{free}^{\text{O-band}}$, $r_{free}^{\text{N-band}}$, and $r_{free}^{\text{M-band}}$ in the gas-filled hohlraum and compare them with the experimental results and the FCI2 simulations. For comparison, the simulations of the empty hohlraum are also presented. As shown, from the LARED-H simulations, the wall plasma expansion in the gas-filled hohlraum is much slower than that in the empty hohlraum. Obviously, the LARED-H simulations agree well with the experiments for all three bands when it is shorter than 2 ns, at which the main laser pulse falls around to its half maximum. However, there is some disagreement after 2.3 ns when the main pulse falls rapidly, especially for the N-band and the M-band. From Figure 13, compared to the experimental results and the FCI2 simulations, the N-band emission region after 2.3 ns moves much slower while the M-band moves much faster from the LARED-H.

In Figure 14, we compare the simulated temporal relative displacements z_I at $f_e = 0.07$ with the experimental observations for the gas-filled hohlraum. As shown, the simulations from LARED-H agree with the observations in general, but there are some differences in detail. From the experiments, v_I is almost the same, around 40 μm/ns, for whole observation time. However, from the LARED-H simulations, z_I has little change within the first 1.5 ns before the main laser pulse reaches its peak, then z_I moves with 43 μm/ns between 1.5 ns and 1.8 ns, and with 98 μm/ns after 1.8 ns when the laser pulse falls rapidly.

SUMMARY

We have studied the influence of f_e on hohlraum plasmas by using the LARED-H simulations and proposed a method to experimentally determine f_e via the motion of the M-band emission region in Au hohlraum. We have simulated the wall and laser spot motion experiments done by Huser *et al.* (2009) by taking different f_e. From our simulations, the limited free streaming flux may dominate the heat conduction in the regions with steep temperature gradient, which are important X-ray emission regions. As a result of our study, the motion of the M-band emission region is sensitive to the f_e when the limited free streaming flux dominates the heat conduction of the wall plasma expansion region, and one can determine f_e via the motion of the M-band emission region.

In general, the LARED-H simulations agree well with the experimental results when f_e is taken as 0.07 for both empty hohlraum and gas-filled hohlraum used in Huser's (2009) experiments. However, there are also some remarkable deviations from the observations, such as the motion of the N-band emissions in the overcritical region and the emission behaviors after 2.3 ns in both empty and gas-filled hohlraums. It is possible that we may have some problems in simulating the hohlraums when laser pulse falls rapidly and hohlraum becomes cold. To understand the disagreements between the simulations and the observations, we will have an experiment for measuring the motion of X-ray emissions on the SG-III prototype laser facility in near future.

ACKNOWLEDGMENT

This work was supported by the National Natural Science Foundation of China, Grant No. 11105014.

REFERENCES

Atzeni, S. & Meyer-Ter-Vehn, J. (2004). *The Physics of Inertial Fusion*. Oxford: Clarendon Press.

Buresi, E., Coutant, J., Dautray, R., Decroisette, M., Dubourgel, B., Guillaneux, P., Launspach, J., Nelson, P., Patou, C., Reisse, J.M. & Watteau, J.P. (1986). Laser program development at CEL-V: Overview of recent experimental results. *Laser Part. Beams* **4**, 531–544.

Cohen, R.S., Spizer, L. & Routly, P.M. (1950). The electrical conductivity of an ionized gas. *Phys. Rev.* **80**, 230–238.

Colombant, D.G., Manheimer, W.M. & Busquet, M. (2005), Test of models for electron transport in laser produced plasmas. *Phys. Plasmas* **12**, 072702–072715.

Cook, R.C., Kozioziemski, B.J., Nikroo, A., Wilkens, H.L., Bhandarkar, S., Forsman, A.C., Haan, S.W., Hoppe, M.L., Huang, H., Mapoles, E., Moody, J.D., Sater, J.D., Seugling, R.M., Stephens, R.B., Takagi, M. & Xu, H.W. (2008). National Ignition Facility target design and fabrication. *Laser Part. Beams* **26**, 479–487.

Gupta, N.K. & Godwal, B.K. (2001). Effects of various parameters on numerical simulations of inertial confinement fusion hohlraum and radiation hydrodynamics. *Laser Part. Beams* **19**, 259–265.

Haan, S.W., Lindl, J.D., Callahan, D.A., Clark, D.S., Salmonson, J.D., Hammel, B.A., Atherton, L.J., Cook, R.C., Edwards, M.J., Glenzer, S., Hamza, A.V., Hatchett, S.P., Herrmann,

https://doi.org/10.1017/S0263034612000225 Published online by Cambridge University Press

M.C., Hinkel, D.E., Ho, D.D., Huang, H., Jones, O.S., Kline, J., Kyrala, G., Landen, O.L., MacGowan, B.J., Marinak, M.M., Meyerhofer, D.D., Milovich, J.L., Moreno, K.A., Moses, E.I., Munro, D.H., Nikroo, A., Olson, R.E., Peterson, K., Pollaine, S.M., Ralph, J.E., Robey, H.F., Spears, B.K., Springer, P.T., Suter, L.J., Thomas, C.A., Town, R.P., Vesey, R., Weber, S.V., Wilkens, H.L. & Wilson, D.C. (2011). Point design targets, specifications, and requirements for the 2010 ignition campaign on the National Ignition Facility. *Phys. Plasmas* **18**, 051001–051047.

Huo, W.Y., Lan, K., Gu, P.J., Yong, H. & Zeng, Q.H. (2012). Electron heat conduction under non-Maxwellian distribution in hohlraum simulation. *Phys. Plasmas* **19**, 012313–012319.

Huo, W.Y., Ren, G., Lan, K., Li, X., Wu, C., Li, Y., Zhai, C., Qiao, X., Meng, X., Lai, D., Zheng, W., Gu, P., Pei, W., Li, S., Yi, R., Song, T., Jiang, X., Yang, D., Jiang, S. & Ding, Y. (2010). Simulation study of Hohlraum experiments on SGIII-prototype laser facility. *Phys. Plasmas* **17**, 123114–123120.

Huser, G., Courtois, C. & Monteil, M.-C. (2009). Wall and laser spot motion in cylindrical hohlraums. *Phys. Plasmas* **16**, 032703–032702.

Kline, J.L., Glenzer, S.H., Olson, R.E., Suter, L.J., Widmann, K., Callahan, D.A., Dixit, S.N., Thomas, C.A., Hinkel, D.E., Williams, E.A., Moore, A.S., Celeste, J., Dewald, E., Hsing, W.W., Warrick, A., Atherton, J., Azevedo, S., Beeler, R., Berger, R., Conder, A., Divol, L., Haynam, C.A., Kalantar, D.H., Kauffman, R., Kyrala, G.A., Kilkenny, J., Liebman, J., Le Pape, S., Larson, D., Meezan, N.B., Michel, P., Moody, J., Rosen, M.D., Schneider, M.B., Van Wonterghem, B., Wallace, R.J., Young, B.K., Landen, O. L. & MacGowan, B.J. (2011). Observation of high soft x-ray drive in large-scale hohlraums at the national ignition facility. *Phys. Rev. Lett.* **106**, 085003–085006.

Lan, K., Fill, E. & Meyer-ter-Vehn, J. (2004). Photopumping of XUV lasers by XFEL radiation. *Laser Part. Beams* **22**, 261–266.

Lan, K., Gu, P., Ren, G., Li, X., Wu, C., Huo, W., Lai, D. & He, X.T. (2010). An initial design of hohlraum driven by a shaped laser pulse. *Laser Part. Beams* **28**, 421–427.

Li, Y.S., Huo, W.Y. & Lan, K. (2011). A novel method for determining the M-band fraction in laser-driven gold hohlraums. *Phys. Plasmas* **18**, 022701–022705.

Li, X., Lan, K., Meng, X., He, X., Lai, D. & Feng, T. (2010). Study on Au + U + Au sandwich Hohlraum wall for ignition targets. *Laser Part. Beams* **28**, 75–81.

Lindl, J.D., (1995). Development of the indirect-drive approach to inertial confinement fusion and the target physics basis for ignition and gain. *Phys. Plasmas* **2**, 3933–4024.

Lindl, J.D., Amendt, P., Berger, R.L., Glendinning, S.G., Glenzer, S.H., Haan, S.W., Sunahara, A., Delletrez, J.A., Stoeckl, C., Short, R.W. & Skupsky, S. (2003). Time-dependent electron thermal flux inhibition in direct-drive laser implosions. Phys. *Rev. Lett.* **91**, 095003–095006.

Lindl, J.D. & Moses, E.I. (2011). Special topic: Plans for the National Ignition Campaign (NIC) on the National Ignition Facility (NIF): On the threshold of initiating ignition experiments. *Phys. Plasmas* **18**, 050901–050902.

Luciani, J.F., Mora, P. & Virmont, J. (1983). Nonlocal heat transport due to steep temperature gradients. *Phys. Rev. Lett.* **51**, 1664–1667.

Malone, R.C., McCrory, R.L. & Morse, R.L. (1975). Indications of strongly flux-limited electron thermal conduction in laser-target experiments. *Phys. Rev. Lett.* **34**, 721–724.

Marinak, M.M., Tipton, R.E., Landen, O.L., Murphy, T.J., Amendt, P., Haan, S.W., Hatchett, S.P., Keane, C.J., McEachern, R. & Wallace, R. (1996). Three-dimensional simulations of Nova high growth factor capsule implosion experiments. *Phys. Plasmas* **3**, 2070–2076.

Orlov, N.Yu., Denisov, O.B., Rosmej, O.N., Schaefer, D., Nisius, Th., Wilhein, Th., Zhidkov, N., Kunin, A., Suslov, N., Pinegin, A., Vatulin, V. & Zhao, Y. (2011). Theoretical and experimental studies of material radiative properties and their applications to laser and heavy ion inertial fusion. *Laser Part. Beams* **29**, 69–80.

Pei, W.B. (2007). The construction of simulation algorithms for laser fusion. *Commun. Comput. Phys.* **2**, 255–270.

Rosen, M.D. & Nuckolls, J.H. (1979). Exploding pusher performance — A theoretical model. *Phys. Fluids* **22**, 1393–1396.

Rosen, M.D., Scott, H.A., Hinkel, D.E., Williams, E.A., Callahan, D.A., Town, R.P.J., Divol, L., Michel, P.A., Kruer, W.L., Suter, L.J., London, R.A., Harte, J.A. & Zimmerman, G.B. (2011). The role of a detailed configuration accounting (DCA) atomic physics package in explaining the energy balance in ignition-scale hohlraums Review. *High Energy Density Phys.* **7**, 180–190.

Seifter, A., Kyrala, G.A., Goldman, S.R., Hoffman, N.M., Kline, J.L. & Batha, S.H. (2009). Demonstration of symcaps to measure implosion symmetry in the foot of the NIF scale 0.7 hohlraums. *Phys. Plasmas* **27**, 123–127.

Serduke, F.J.D., Minguez, E., Davidson, S.J. & Iglesias, C.A. (2000). WorkOp-IV summary: Lessons from iron opacities. *J. Quant. Spectro. & Rad. Trans.* **65**, 527–541.

Shurtz, G.P., Nicolai, P. & Busquet, M. (2000). A nonlocal electron conduction model for multidimensional radiation hydrodynamics codes. *Phys. Plasmas* **7**, 4238–4249.

Spitzer, JR.L. & Härm, R. (1953). Transport Phenomena in a Completely Ionized Gas. *Phys. Rev.* **89**, 977–981.

Zimmerman, G.B. & Kruer, W.L. (1975). Numerical Simulation of Laser-Initiated Fusion. *Comments Plasma Phys. Control. Fusion* **2**, 51.